Journal of Solid Mechanics Vol. 9, No. 1 (2017) pp. 63-85

Thermo-Elastic Analysis of Non-Uniform Functionally Graded Circular Plate Resting on a Gradient Elastic Foundation

A. Behravan Rad *

Engineering Department ,Zamyad Company,15Km Karaj Old Road, P.O 1386183741, Tehran, Iran

Received 20 September 2016; accepted 14 December 2016

ABSTRACT

Present paper is devoted to stress and deformation analyses of heated variable thickness functionally graded (FG) circular plate with clamped supported, embedded on a gradient elastic foundation and subjected to non-uniform transverse load. The plate is coupled by an elastic medium which is simulated as a Winkler- Pasternak foundation with gradient coefficients in the radial and circumferential directions during the plate deformation. The temperature distribution is assumed to be a function of the thickness direction. The governing state equations are derived in terms of displacements and temperature based on the 3D theory of thermo-elasticity. These equations are solved using a semi-analytical method to evaluate the deformation and stress components in the plate. Material properties of the plate except the Poisson's ratio are assumed to be graded continuously along the thickness direction according to an exponential distribution. A parametric study is accomplished to evaluate the effects of material heterogeneity indices, foundation parameters, temperature difference between the top and bottom surfaces of the plate and thickness to radius ratio on displacements and stresses. The results are reported for the first time and the new results can be used as a benchmark solution for the future researches.

Keywords : Functionally graded; Circular plate; Gradient foundation; Thermo-mechanical; Semi-analytical; Non-uniform.

1 INTRODUCTION

THE functionally graded materials (FGMs) are a novel class of engineering materials, which those thermo-mechanical properties vary continuously in a specific direction. Based on this characteristic two types of graded circular plates are reported in the literature. Some types are transversely graded plates and the other types are radially graded plates. FGMs have received considerable attention by researchers in recent years because those novel properties enable them to be widely used in many scientific and engineering disciplines, such as aerospace, vehicles, optics, electronics, mechanical, nuclear and biomedical engineering.

Plate resting on an elastic foundation is a classical topic in engineering. Practical examples of these are airport run-ways, foundation of storage tanks and silos, driven plates of a friction clutch, Vehicle brake disk on friction pads, Nano-plates embedded in an elastic matrix or resting on an elastomeric substrate and biological organs resting on artificial medium.

*Corresponding author.
E-mail address: abehravanrad@aol.com (A. Behravanrad).

There are two approaches for designing these typical applications: the constant-life and constant-pressure approaches. Therefore, the distributed forces exerted by the foundation may not be uniform even for a uniform displacement field. Subsequently, as a general case, the stiffness of the foundation may not be uniform.

Some researchers have investigated thermo-elastic behavior of the FG circular plates, employing the plate theories. For example, Reddy et al. [1] reported some closed-form expressions to analyze the bending of transversely graded annular and circular plates under the effect of symmetric loading. Najafizadeh and Heydari [2] treated the buckling of FGM plates under the effect of thermo-mechanical loads based on the Von-Karma non-linearity and Reddy's third order thick plate theory. They assumed that the mechanical properties of FG plates are graded along the plate thickness direction according to power low form. Based on this nonlinear theory Ma and Wang [3] investigated the axisymmetric large deflection bending of a FG circular plate under mechanical, thermal and combined thermal-mechanical loading, they used the shooting method to numerically solve the problem. Khorshidvand et al. [4] studied the thermal buckling of FG circular plates integrated with piezoelectric layers under the uniform, linear and nonlinear temperature variation and constant voltage. They applied the energy method with the use of calculus of variations based on the classical plate theory to obtain the critical buckling temperature. Kiani and Eslami [5] studied analytically the buckling of heated FG annular plates resting on a conventional Pasternak-type elastic foundation based on the classical plate theory under the effect of various thermal loads. They considered distribution of thermo-mechanical properties in the plate thickness according to power law function. Gaikwad [6] studied thermo elastic deformation of a thin hollow circular disk due to the partially distributed and axisymmetric heat supply on the upper surface, and analyzed thermo-elastic deformations analytically based on Kirchhoff-Love's hypothesis and introduced an integral transforms method to analyze the temperature field. Golmakani and Kadkhodayan [7] investigated the axisymmetric bending and stretching of circular and annular functionally graded plates with variable thicknesses under combined thermal-mechanical loading based on the first-order shear deformation theory and employing the dynamic relaxation (DR) method to solve the governing equations. Recently, Fallah and Noseir [8] presented closed – form solutions for analysis of thermo-mechanical behavior of FG circular sector plates based on the first–order shear theory of plates.

A number of numerical approaches have been employed to study the thermo-elastic problems of FG circular plates, among which finite element method and differential quadrature rule based on certain simplified plate theories and 2D thermo-elasticity have been used frequently. For instance, Gunes and Reddy [9] studied the behavior of geometrically nonlinear FG circular plates under the effect of mechanical and thermal loads by employing finite element method. In this study the Green-Lagrange strain tensor with all its terms is considered. Prakash and Ganapathi [10] performed an asymmetric study on vibration and thermal buckling of FGM circular plates by using finite element method. Gomshei and abbasi [11] developed a finite element formulation for analyzing the axisymmetric thermal buckling of variable thickness FG annular plates subjected to arbitrary distribution thermal loads along the plate radial direction. Afsar and Go [12] applied the finite element method to analyze the thermo elastic field in a thin FG circular disk subjected to thermal load and an inertia force due to rotation of the disk. They considered the thermo-mechanical properties of the plate constituents graded in radial direction and formulated the governing equation of an axisymmetric problem based on the two dimensional thermo-elastic theories. Leu and Chien [13] investigated the thermo-elastic behavior of FG rotating disks with variable thickness and including a non-uniform heat source by utilizing finite element method.

Safaeian et al. [14] applied the differential quadrature (DQ) method to present the effects of thermal environment and temperature dependence of the material properties on axisymmetric bending of FG circular and annular plates. Based on the first order shear deformation theory and using DQ method, Malekzadeh et al. [15] investigated the free vibration problem of FG annular plates supported by two-parameter elastic foundation in thermal environment. Sepahi et al. [16] treated the buckling and post buckling behaviors of heated annular FG plates by utilizing DQ method. In this analysis, the material properties are assumed to be temperature dependent and graded in the radial direction. In other study, Sepahi et al. [17] investigated the effect of three-parameter elastic foundations and thermo-mechanical load on the axisymmetric large deflection of a simply-supported annular FG plate.

It is evident that results of the three-dimensional theory of elasticity are exact and more accurate than those of the plate theories which are indeed two-dimensional theories whose dependence on the transverse coordinate is prescribed. Therefore some researchers reported the static, vibration and thermo-elastic behaviors of FG circular plates based on this theory. According to 3D elasticity theory and assuming the material properties to vary with an exponential distribution in transverse direction, Jabbari et al. [18] developed an analytical solution for steady state thermo-elastic problem of simply supported FG circular plate under axisymmetric thermal and mechanical loads. Nie and Zhong [19] presented a semi-analytical (State space method and one dimensional differential quadrature rule) solution for three-dimensional free and forced vibration analyses of functionally graded circular plate with

various boundary conditions. By using direct displacement method, Yu Li et al. [20] carried out an analytical solution to investigate the axisymmetric thermo-elastic behavior of FG circular plate under thermal load. The author [21] discussed the static behavior of unidirectional FG circular plates resting on elastic foundation under the effect of axisymmetric transverse load by using semi-analytical method. In addition to this analysis, assuming exponential type of property distribution in both transverse and radial directions, Behravan Rad and Alibeigloo [22] investigated the static behavior of two directional FG circular plates resting on elastic foundation under the effect of axisymmetric transverse load. Recently the author developed the differential equation of interaction between foundation-structure to a linear elastic foundation with gradient coefficients, and analyzed the static response of variable thickness multidirectional FG circular and annular plates supported by variable elastic foundation (Winkler-Pasternak type) to compound mechanical loads [23].

The foregoing brief review reveals that very limited papers have been published on the thermo-elastic analysis of FG circular plates. Three dimensional bending and stress analysis of variable thickness FG circular plate resting on gradient elastic foundation under the effects of thermal and mechanical loads has not been performed before. Present research is devoted to exact deformation and stress analyses of variable thickness FG circular plate embedded on non-uniform two-parameter Winkler-Pasternak elastic foundation. Material properties are assumed to be graded in the thickness direction according to an exponential distribution. The formulations are based on the three-dimensional theory of thermo-elasticity. A semi-analytical approach, which makes use of the state space method and the one-dimensional differential quadrature rule, is used to extract the numerical results.

The novelties of the present study can be outlined as follows:

1. Presenting a semi-analytical solution for thermo-elastic analysis of variable thickness FG circular plate with complicated boundary conditions.
2. Demonstrating the thermo-elastic behavior of non-uniform FG circular plate under the effect of general tractions (asymmetric transverse load and variable plate-foundation interaction), for the first time.
3. Extracting new differential equation for the gradient elastic foundation.
4. Illustrating the effect of foundation parameters and foundation gradient indices on thermo-elastic behavior of variable thickness FG circular plate, for the first time.
5. Presenting quite new and interesting stress and deformation results for the FG circular plate.

2 MATHEMATICAL FORMULATION

2.1 Basic equations

Fig.1 illustrates a functionally graded circular plate with variable thickness $h(r)$ and outer radius a, embedded on a gradient elastic foundation. The plate is clamped supported at circumferential edge and subjected to non-uniform transverse load $p(r,\theta,z)$ and uniform temperatures T_1, T_2 over the bottom and top surfaces of the plate, respectively.

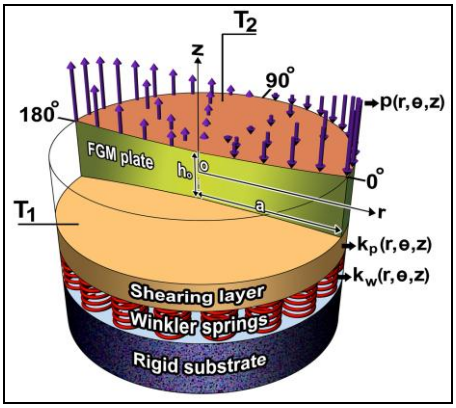

Fig.1
Geometry of the problem and coordinate system.

The FG plate is transversely isotropic with constant Poisson's ratio (ν) and the other material properties with the exponential distribution along the thickness direction are as follows:

$$E(z) = E_0 \exp\left(n_1 \left(\frac{z}{h} + \frac{1}{2} \right) \right) \tag{1}$$

$$\alpha(z) = \alpha_0 \exp\left(n_2 \left(\frac{z}{h} + \frac{1}{2} \right) \right) \tag{2}$$

$$K(z) = K_0 \exp\left(n_3 \left(\frac{z}{h} + \frac{1}{2} \right) \right) \tag{3}$$

where E_0, α_0, K_0 are the Young's module, thermal expansion and thermal conductivity of the plate material at the bottom surface, respectively. n_1, n_2, n_3 are the parameters indicating the trends of the plate material properties gradient.

The thickness profile of the plate is assumed to vary in radius direction according to:

$$h(r) = h_0 \left(1 + \alpha_1 \left(\frac{r}{a} \right) + \alpha_2 \left(\frac{r}{a} \right)^2 \right) \tag{4}$$

where h_0 is the thickness at the center of the plate and α_1, α_2 are the plate geometry variation coefficients. The external load on the top surface of the plate is assumed to vary in radial and circumferential directions according to:

$$p(r, \theta, z) = p_0 \left(1 + p_1 \left(\frac{r}{a} \right) + p_2 \left(\frac{r}{a} \right)^2 \right) \cos(\theta) \tag{5}$$

where p_0 denotes the value of external load at the center of the plate, p_1 and p_2 denote the load variation coefficients.

The equilibrium equations in the absence of body forces are

$$\sigma_{r,r} + r^{-1}\tau_{r\theta,\theta} + \tau_{rz,z} + r^{-1}(\sigma_r - \sigma_\theta) = 0 \tag{6a}$$

$$\tau_{r\theta,r} + r^{-1}\sigma_{\theta,\theta} + \tau_{\theta z,z} + 2r^{-1}\tau_{r\theta} = 0 \tag{6b}$$

$$\tau_{rz,r} + r^{-1}\tau_{\theta z,\theta} + \sigma_{z,z} + r^{-1}\tau_{rz} = 0 \tag{6c}$$

where $\sigma_r, \sigma_\theta, \sigma_z, \tau_{\theta z}, \tau_{rz}, \tau_{r\theta}$ are the stress components and the comma denotes differentiation with respect to the indicated variable.

The mechanical displacements and stresses are assumed in the following form:

$$u(r, \theta, z) = u(r, z)\cos(\theta) \tag{7a}$$

$$v(r, \theta, z) = v(r, z)\sin(\theta) \tag{7b}$$

$$w(r, \theta, z) = w(r, z)\cos(\theta) \tag{7c}$$

$$\sigma_r(r, \theta, z, n_1, n_2) = \sigma_r(r, z, n_1, n_2)\cos(\theta) \tag{7d}$$

$$\sigma_\theta(r, \theta, z, n_1, n_2) = \sigma_\theta(r, z, n_1, n_2)\cos(\theta) \tag{7e}$$

$$\sigma_z(r, \theta, z, n_1, n_2) = \sigma_z(r, z, n_1, n_2)\cos(\theta) \tag{7f}$$

$$\tau_{rz}(r, \theta, z, n_1) = \tau_{rz}(r, z, n_1)\cos(\theta) \tag{7g}$$

$$\tau_{\theta z}(r,\theta,z,n_1)=\tau_{\theta z}(r,z,n_1)\sin(\theta) \tag{7h}$$

$$\tau_{r\theta}(r,\theta,z,n_1)=\tau_{r\theta}(r,z,n_1)\sin(\theta) \tag{7i}$$

where u,v,w are displacement components in the r,θ and z directions.

The kinematic equations are:

$$\varepsilon_r=u(r,\theta,z)_{,r} \tag{8a}$$

$$\varepsilon_\theta=r^{-1}v(r,\theta,z)_{,\theta}+r^{-1}u \tag{8b}$$

$$\varepsilon_z=w(r,\theta,z)_{,z} \tag{8c}$$

$$\gamma_{rz}=u(r,\theta,z)_{,z}+w(r,\theta,z)_{,r} \tag{8d}$$

$$\gamma_{\theta z}=r^{-1}w(r,\theta,z)_{,\theta}+v(r,\theta,z)_{,z} \tag{8e}$$

$$\gamma_{r\theta}=r^{-1}u(r,\theta,z)_{,\theta}+v(r,\theta,z)_{,r}-r^{-1}v(r,\theta,z) \tag{8f}$$

where $\varepsilon_r,\varepsilon_\theta,\varepsilon_z,\gamma_{\theta z},\gamma_{rz},\gamma_{r\theta}$ are the strain components.

The constitutive relations from 3-D theory of uncoupled thermo-elasticity are:

$$\sigma_r=\frac{E(z)}{(1+v)(1-2v)}\left((1-v)u(r,\theta,z)_{,r}+vr^{-1}(v(r,\theta,z)_{,\theta}+u(r,\theta,z))+vw(r,\theta,z)_{,z}\right)-\frac{E(z)\alpha(z)}{1-2v}T(z) \tag{9a}$$

$$\sigma_\theta=\frac{E(z)}{(1+v)(1-2v)}\left(vu(r,\theta,z)_{,r}+(1-v)r^{-1}u(r,\theta,z)+vw(r,\theta,z)_{,z}\right)-\frac{E(z)\alpha(z)}{1-2v}T(z) \tag{9b}$$

$$\sigma_z=\frac{E(z)}{(1+v)(1-2v)}\left(vu(r,\theta,z)_{,r}+vr^{-1}u(r,\theta,z)+(1-v)w(r,\theta,z)_{,z}\right)-\frac{E(z)\alpha(z)}{1-2v}T(z) \tag{9c}$$

$$\tau_{rz}=\frac{E(z)}{2(1+v)}\left(u(r,\theta,z)_{,z}+w(r,\theta,z)_{,r}\right) \tag{9d}$$

$$\tau_{\theta z}=\frac{E(z)}{2(1+v)}\left(r^{-1}w(r,\theta,z)_{,\theta}+v(r,\theta,z)_{,z}\right) \tag{9e}$$

$$\tau_{r\theta}=\frac{E(z)}{2(1+v)}\left(v(r,\theta,z)_{,r}-r^{-1}v(r,\theta,z)+r^{-1}u(r,\theta,z)_{,\theta}\right) \tag{9f}$$

The governing equation for the steady state one-dimensional heat conduction equation, in the absence of heat source is

$$\left(k(z)T_{,z}\right)_{,z}=0 \tag{10}$$

The thermo-mechanical edge and boundary conditions are

$$u(r,\theta,z)=0,\quad v(r,\theta,z)=0,\quad w(r,\theta,z)=0,\quad T(a,z)=0\qquad at\ \ r=a \tag{11}$$

Regularity conditions on the center of the plate:

$$u(r,\theta,z)=0,\quad v(r,\theta,z)=0,\quad w(r,\theta,z)_{,r}=0,\quad T(0,z)_{,r}=0\qquad at\ \ r=0 \tag{12}$$

$$\sigma_z=p_f(r,\theta,z)=0,\quad \tau_{z\theta}=0,\quad \tau_{rz}=0,\quad T(r,0)=T_1\qquad at\ \ z=-h/2 \tag{13}$$

$$\sigma_z=-p(r,\theta,z)=0,\quad \tau_{z\theta}=0,\quad \tau_{rz}=0,\quad T(r,h)=T_2\qquad at\ \ z=h/2 \tag{14}$$

where $p_f, p(r,\theta,z)$ are the plate–foundation interaction and external mechanical load, respectively.

In order to simplify calculations and transform from physical domain to a normalized computational domain, the following non-dimensional quantities are introduced:

$$U=\frac{u(r,\theta,z)}{h(r)},\quad V=\frac{v(r,\theta,z)}{h(r)},\quad W=\frac{w(r,\theta,z)}{h(r)},\quad \eta=\frac{r}{a},\quad \xi=\frac{z(r)}{h(r)},\quad s=\frac{h}{a},\quad 0\le\xi=\xi+0.5\le 1,\quad 0\le\eta\le 1 \tag{15a}$$

$$\sigma_\eta=\frac{\sigma_r}{Y},\quad \sigma_\Theta=\frac{\sigma_\theta}{Y},\quad \sigma_\xi=\frac{\sigma_z}{Y},\quad \tau_{\eta\xi}=\frac{\tau_{rz}}{Y},\quad \tau_{\Theta\xi}=\frac{\tau_{\theta z}}{Y},\quad \tau_{\eta\Theta}=\frac{\tau_{r\theta}}{Y},\quad \bar{T}=\alpha_3 T,\quad \alpha_3=10^{-6}\ /^{\circ}c \tag{15b}$$

where $Y=1Gpa$.

By considering the Eqs.(1),(2),(6),(9) and (15a), the normalized form of the governing equations in terms of displacements and temperature in the bottom surface of the plate can be obtained as:

$$\begin{aligned}&U_{,\varsigma\varsigma}=-\left(\frac{2(1-\nu)}{1-2\nu}\right)(s)^2\beta_1^2\left(U_{,\eta\eta}+\left(\frac{1}{\eta}+2\beta_2\right)U_{,\eta}+\left(\frac{\beta_2}{\eta}+\beta_3-\frac{1}{\eta^2}\right)U\right)+(s)^2\beta_1^2\frac{1}{\eta^2}U-\\&\frac{2\nu}{1-2\nu}(s)^2\beta_1^2\frac{1}{\eta}\left(V_{,\eta}+(\beta_2)V\right)+\frac{2(1-\nu)}{1-2\nu}(s)^2\beta_1^2\frac{V}{\eta^2}-(s)^2\beta_1^2\left(\frac{1}{\eta}V_{,\eta}+\left(\frac{\beta_2}{\eta}-\frac{1}{\eta^2}\right)V\right)-n_1 s\beta_1(W_{,\eta}+\beta_2 W)-\\&n_1U_{,\varsigma}-\left(\frac{2\nu}{1-2\nu}\right)s\beta_1\left(W_{,\eta\varsigma}+\left(\beta_2+\frac{1}{\eta}\right)W_{,\varsigma}\right)+\left(\frac{2\nu}{(1-2\nu)}\right)\frac{s\beta_1}{\eta}W_{,\varsigma}-s\beta_1(W_{,\eta\varsigma}+\beta_2W_{,\varsigma})\end{aligned} \tag{16a}$$

$$\begin{aligned}&V_{,\varsigma\varsigma}=\frac{2\nu}{1-2\nu}(s)^2\frac{\beta_1^2}{\eta}\left(U_{,\eta}+\beta_2U\right)+\frac{2(1-\nu)}{1-2\nu}(s)^2\beta_1^2\frac{U}{\eta^2}+(s)^2\beta_1^2\left(\frac{1}{\eta}U_{,\eta}+\left(\frac{\beta_2}{\eta}+\frac{U}{\eta^2}\right)\right)+\\&\frac{2(1-\nu)}{(1-2\nu)}(s)^2\beta_1^2\frac{V}{\eta^2}-(s)^2\beta_1^2\left(V_{,\eta\eta}+\left(2\beta_2+\frac{1}{\eta}\right)V_{,\eta}+\left(\beta_2+\beta_3-\frac{1}{\eta^2}\right)V\right)+n_1s\beta_1\frac{W}{\eta}-n_1V_{,\varsigma}+\frac{1}{\eta}\left(\frac{1}{1-2\nu}\right)W_{,\varsigma}\end{aligned} \tag{16b}$$

$$\begin{aligned}&W_{,\varsigma\varsigma}=-n_1\left(\frac{\nu}{1-\nu}\right)s\beta_1\left(U_{,\eta}+\left(\beta_2+\frac{1}{\eta}\right)U\right)-n_1\left(\frac{\nu}{1-\nu}\right)s\beta_1\frac{V}{\eta}-\left(\frac{1-2\nu}{2(1-\nu)}\right)s^2\beta_1^2\\&\left(W_{,\eta\eta}+\left(\frac{1}{\eta}+2\beta_2\right)W_{,\eta}+\left(\beta_3+\frac{\beta_2}{\eta}-\frac{1}{\eta^2}\right)\right)-\left(\frac{\nu}{(1-\nu)}\right)s\beta_1\left(U_{,\eta\varsigma}+\left(\beta_2+\frac{1}{\eta}\right)\frac{1}{\eta}U_{,\varsigma}\right)-\\&\frac{1}{2(1-\nu)}s\beta_1\frac{V_{,\varsigma}}{\eta}-n_1W_{,\varsigma}+\left(\frac{1+\nu}{1-\nu}\right)\left(\frac{\alpha_0}{\alpha_3}\right)\left((n_1+n_2)\bar{T}+\bar{T}_{,\xi}\right)\end{aligned} \tag{16c}$$

where

$$\beta_1=\left(1+\alpha_1\left(\frac{\eta-b/a}{1-b/a}\right)+\alpha_2\left(\frac{\eta-b/a}{1-b/a}\right)^2\right),\ \beta_2=\frac{1}{(1-b/a)}\left(\alpha_1+2\alpha_2\left(\frac{\eta-b/a}{1-b/a}\right)\right)/\beta_1,\ \beta_3=2\alpha_2/\beta_1(1-b/a)^2$$

2.2 The plate-foundation interaction

It is assumed that, the two parameter elastic foundation is perfect, frictionless, attached to the plate, non-uniform, asymmetric, and isotropic, that is, $k_{pr}=k_{p\theta}=k_p$. In the referred coordinate system the interface pressure $p_f(r,\theta,z)$ between the structure and a non-uniform foundation may be expressed mathematically as follows:

$$p_f(r,\theta,z)=k_w(r,\theta,z)w_b-r^{-1}\left(rk_p(r,\theta,z)\frac{\partial w_b}{\partial r}\right)_{,r}-r^{-2}\left(k_p(r,\theta,z)\frac{\partial w_b}{\partial\theta}\right)_{,\theta} \tag{17}$$

where $p_f(r,\theta,z)$ denotes the foundation reaction per unit area and w_b is the deflection of the bottom surface of the plate. $\mathrm{k_w(r,\theta,z)}$, $\mathrm{k_p(r,\theta,z)}$ are the coordinate dependent Winkler-Pasternak coefficients and can be expressed as:

$$k_w(r,\theta,z)=k_{wbo}\left(1+f_1(r/a)+f_2(r/a)^2\right)\cos(\theta),\ \ k_p(r,\theta,z)=k_{pbo}\left(1+f_1(r/a)+f_2(r/a)^2\right)\cos(\theta) \tag{18}$$

where $k_{wbo}(N/m^3), k_{pbo}(N/m)$ are the elastic coefficients of Winkler-Pasternak foundation at the center of bottom surface of the plate.

3 SOLUTION TECHNIQUE

This study only considers the uncoupled thermo-elastic problem for a functionally graded circular plate. Therefore, the steady state heat conduction equation shown in Eq. (10) can be solved individually by direct integrating. The temperature distribution across the plate thickness can be obtained as [3,7].

$$T(\xi)=T_1+(T_1-T_2)\int_{-\frac{h}{2}}^{\varsigma}\frac{d\varsigma}{k(\varsigma)}\Bigg/\int_{-\frac{h}{2}}^{\frac{h}{2}}\frac{d\varsigma}{k(\varsigma)} \tag{19}$$

To solve the governing differential equations appeared in Eq. (16) a semi-analytical approach is employed. This method gives an analytical solution along the thickness direction (z-direction) by using the state space method (SSM) and a numerical solution in the radial direction of the plate by applying one dimensional differential quadrature (DQ) rule to approximate the stress and deformation components. By using this method the governing differential equations is transformed from physical domain to a normalized computational domain and the special derivatives are discretized by applying the one dimensional differential quadrature rule as an efficient and accurate numerical tool. The obtained linear eigenvalue system in terms of the displacements and temperature is solved and the thermo-elastic behavior of the plate under described boundary conditions is analyzed.

3.1 DQM procedure and its application

The DQ method is a numerical technique which divides the continuous domain in to a set of discrete points and replaces the derivative of an arbitrary unknown function with the weighted summation of the functions values in the discretized points. Therefor, the principle of DQ rule can be stated as follow: for a continuous function $g(r)$ defined in an interval $r\in[0,1]$, its nth-order derivative with respect to argument r at an arbitrary given point r_i can be approximated by a linear sum of the weighted function values of $g(r)$ in the whole domain [24]. The mathematical presentation of the method is

$$\frac{\partial^{(n)} g(r_i)}{\partial r^n} = \sum_{j=1}^{N} A_{ij}^{(n)} g(r_j) \qquad i = 1,2,...,N \quad and \quad n = 1,2,...,N-1 \tag{20}$$

where $A_{ij}^{(n)}$ is the weighting coefficients matrix of the nth-derivative determined by the coordinates of the sample points r_i and N is the number of the grid points in the radial direction. There are different ways for calculating the weighting coefficient matrix, because different functions may be considered as test functions. In this study a set of Lagrange polynomials are employed as test functions, and to achieve more accuracy the non-uniform grid spacing is considered. Explicit expressions of the first and second derivatives of the weighted coefficients matrices and also criterion to adopt non-uniformly spaced grid points are [25]:

The first order derivative of the weighting coefficients matrix

$$\begin{aligned} A_{ik} &= \frac{\prod_{j=1, j\neq i}^{N} (r_i - r_j)}{(r_i - r_k) \prod_{j=1, j\neq k}^{N} (r_k - r_j)} \qquad i \neq k, \;\; i,k = 1,2,3,...,N \\ A_{ii} &= -\sum_{j=1, j=i}^{N} A_{ij} \qquad i = k, \;\; i = 1,2,3,...,N \end{aligned} \tag{21}$$

The second-order derivative of the weighting coefficients matrix

$$\begin{aligned} A_{ik}^{(2)} &= 2\left[A_{ii} A_{ik} - \frac{A_{ik}}{r_i - r_k} \right] \qquad i \neq k, \;\; i,k = 1,2,3,...,N \\ A_{ii}^{(2)} &= -\sum_{j=1, j=i}^{N} A_{ij}^{(2)} \qquad i = k, \;\; i = 1,2,3,...,N \end{aligned} \tag{22}$$

The Richard-Shu criterion

$$r_i = \frac{1}{2}\left(1 - \cos\left(\frac{(i-1)\pi}{N-1} \right) \right) \qquad i = 1,2,3,...,N \tag{23}$$

The partial derivatives of the unknown displacements U,V,W with respect to η appeared in Eq. (16) after applying the DQ rule at an arbitrary sample point η_i can be expressed as:

$$(U,\eta)_{\eta i} = \sum_{j=1}^{N} A_{ij} U_j \tag{24a}$$

$$(V,\eta)_{\eta i} = \sum_{j=1}^{N} A_{ij} V_j \tag{24b}$$

$$(W,\eta)_{\eta i} = \sum_{j=1}^{N} A_{ij} W_j \tag{24c}$$

$$(U,\eta\eta)_{\eta i} = \sum_{j=1}^{N} A_{ij}^{(2)} U_j \tag{24d}$$

$$(V,\eta\eta)_{\eta i}=\sum_{j=1}^{N}A_{ij}^{(2)}V_j \tag{24e}$$

$$(W,\eta\eta)_{\eta i}=\sum_{j=1}^{N}A_{ij}^{(2)}W_j \tag{24f}$$

$$(U,\eta\varsigma)_{\eta i}=\sum_{j=1}^{N}A_{ij}U_{,\varsigma j} \tag{24g}$$

$$(V,\eta\varsigma)_{\eta i}=\sum_{j=1}^{N}A_{ij}V_{,\varsigma j} \tag{24h}$$

$$(W,\eta\varsigma)_{\eta i}=\sum_{j=1}^{N}A_{ij}W_{,\varsigma j} \tag{24i}$$

The associated edge conditions in discretized points can be written as follows:

$$U_N=0,\quad V_N=0,\quad W_N=0,\quad \bar{T}_N=0,\qquad at\quad \eta=1 \tag{25}$$

Regularity conditions on the center of the plate:

$$U_1=0,\quad V_1=0,\quad W_1=-\sum_{j=2}^{N}\frac{A_{1j}}{(\beta_{21}+A_{11})}W_j,\quad \bar{T}_{,\eta}=0,\qquad at\quad \eta=0 \tag{26}$$

The discretized forms of the boundary conditions at the lower and upper surfaces of the plate, Eqs.(13) and (14) can be written as:

$$at\ \ \varsigma=0,,\qquad (U,\varsigma)_i+s\beta_{1i}\left(\sum_{j=1}^{N}A_{ij}W_j+\beta_{2i}W_i\right)=0 \tag{27a}$$

$$(V,\varsigma)_i-s\frac{\beta_{1i}\cot g(\theta)}{\eta_i}W_i=0 \tag{27b}$$

$$(W,\varsigma)_i+\frac{s\nu}{1-\nu}\beta_{1i}\left(\sum_{j=1}^{N}A_{ij}U_j+\left(\beta_{2i}+\frac{1}{\eta_i}\right)U_i+\frac{tg(\theta)}{\eta_i}V_i\right)-\left(\frac{1+\nu}{1-\nu}\right)\frac{\alpha_0}{\alpha_3}\bar{T}_i=$$

$$\beta_{1i}\left(k_1\beta_{4i}\cos(\theta)W_i-k_2\left(\begin{array}{l}\beta_{4i}\cos(\theta)\left(\sum_{j=2}^{N}A_{i1}^{(2)}\frac{A_{1j}}{A_{11}}\right)W_j\\ +\left(2\beta_{2i}\beta_{4i}+\frac{\beta_{4i}}{\eta_i}+\beta_{5i}\right)\cos(\theta)\left(\sum_{j=2}^{N-1}A_{ij}-\sum_{j=2}^{N-1}A_{i1}-\frac{A_{1j}}{A_{11}}\right)W_j\\ +\left(\begin{array}{l}\left(\beta_{2i}\left(\frac{\beta_{4i}}{\eta_i}+\beta_{5i}\right)+\beta_{3i}\beta_{4i}\right)\cos(\theta)+\\ \left(\beta_{4i}\left(\cos^2(\theta)-\sin^2(\theta)\right)\right)\frac{1}{\eta_i^2}\end{array}\right)W_i\end{array}\right)\right) \tag{27c}$$

$$\overline{T}_i = \overline{T}_1 \qquad (i = 1,2,3,...,N) \tag{27d}$$

where $k_1 = \dfrac{k_{wb0}(1+\nu)(1-2\nu)h}{2(1-\nu)E_b}, k_2 = \dfrac{k_{pb0}(1+\nu)(1-2\nu)}{2(1-\nu)E_b}\dfrac{s}{a}$ are the dimensionless coefficients of the elastic foundation and $\beta_{4i} = \left(1 + f_1\eta_i + f_2\eta_i^2\right), \beta_{5i} = \left(f_1 + 2f_2\eta_i\right)$.

$$at\ \varsigma = 1, \qquad \left(U,\varsigma\right)_i + s\beta_{1i}\left(\sum_{j=1}^{N} A_{ij}W_j + \beta_{2i}W_i\right) = 0 \tag{28a}$$

$$\left(V,\varsigma\right)_i - s\frac{\beta_{1i}\cot g(\theta)}{\eta_i}W_i = 0 \tag{28b}$$

$$\left(W,\varsigma\right)_i + \frac{s\nu}{(1-\nu)}\beta_{1i}\left(\sum_{j=1}^{N} A_{ij}U_j + \left(\beta_{2i} + \frac{1}{\eta_1}\right)U_i + \frac{tg(\theta)}{\eta_i}V_i\right) - \left(\frac{1+\nu}{1-\nu}\right)\frac{\alpha_h}{\alpha_3}\overline{T}_i = \frac{-(1+\nu)(1-2\nu)P_i}{(1-\nu)\exp(n_1)} \tag{28c}$$

$$\overline{T}_i = \overline{T}_2 \qquad (i = 1,2,3,...,N) \tag{28d}$$

3.2 The state space method

Assembling of governing equations appeared in Eq. (16) in a state space notation at all discrete points gives the global state equation in a matrix form as:

$$\left\{\delta_i(\varsigma)\right\}_{,\varsigma} = \left[D_i\right]\left\{\delta_i(\varsigma)\right\} + \left[B_i\right]\left\{t_i(\varsigma)\right\} \tag{29}$$

Here, $\delta_i(\varsigma) = \left[U_i \quad V_i \quad W_i \quad U_{,\varsigma i} \quad V_{,\varsigma i} \quad W_{,\varsigma i}\right]^T$, $t_i(\varsigma) = \left[\overline{T}_{1i} \quad 0 \quad 0 \quad 0 \quad 0 \quad \overline{T}_{,\varsigma i}\right]^T$ are the global state and temperature vectors along the plate thickness at the level of ς, respectively. D_i, B_i are the coefficient matrices at sample points. The elements of these matrices are expressed in Appendix 1.

By considering all edge conditions the Eq. (29) can be denoted as follows:

$$\left[\delta_{ei}(\varsigma)\right]_{,\varsigma} = \left[D_{ei}\right]\left[\delta_{ei}(\varsigma)\right] + \left[B_{ei}\right]\left[t_{ei}(\varsigma)\right] \tag{30}$$

where the subscript '*e*' denotes the modified matrix or unknown vector taking account of the edge conditions.

According to the rules of matrix operation, the general solution to Eq. (30) is:

$$\delta_{ei}(\varsigma) = \exp(\varsigma D_{ei})\delta_{ei}(0) + H_\varsigma \tag{31}$$

where the term H_ξ is the thermal loading vector defined by

$$H_\varsigma = \int_0^\varsigma \exp\left((\varsigma - \tau)D_e\right)B_e(\tau)t(\tau)d\tau \tag{32}$$

The recent integral is implemented via numerical quadrature in the present study. Eq. (31) establishes the transfer relations from the state vector on the bottom surface to that at an arbitrary plane ς of the plate by the exponential matrix of $\exp(\varsigma D_{ei})$. Setting $\varsigma = 1$ in Eq. (32) gives

$$\delta_{ei}(1) = \exp(D_{ei})\delta_{ei}(0) + H_1 \tag{33}$$

where $\exp(D_{ei})$ is the global transfer matrix and H_1 is obtained by setting the upper bound of integration to unity in Eq. (32). $\delta_{ei}(1), \delta_{ei}(0)$ are the values of the state variables at the upper and lower planes of the plate, respectively.

By substituting the boundary conditions presented in Eqs. (27), (28) in to Eq. (33), the following algebraic equations for thermo-elastic analysis can be obtained

$$MX = Q \tag{34}$$

where M is a $6(N-2)\times 6(N-2)$ matrix, Q is a traction vector (mechanical and thermal tractions) and

$$X = \left[U_i(0) \quad V_i(0) \quad W_i(0) \quad U_i(1) \quad V_i(1) \quad W_i(1)\right]^T \quad , \quad (i = 2,3,...,N-1) \tag{35}$$

By solving Eq. (34), all the state parameters at $\varsigma = 0, \varsigma = 1$ are obtained. Eqs. (30) and (9) may be used to calculate the displacement and the stress components of the FG circular plate.

4 THE NUMERICAL RESULTS AND DISCUSSIONS

The first example of the present section is devoted for verification proposes, the next example is performed for temperature field analysis, and the other examples contain new results. The material properties are assumed to vary in the thickness direction of the plate according to Eqs. (1)- (3). The FG plate considered in the examples is assumed to be composed of Aluminum as bottom metal surface and Alumina as top ceramic surface. The material properties of the FGM constituents are taken from [5] and summarized in Table1.

Table1
Mechanical and thermal properties of FG circular plate.

Materials	Young's modulus E(GPa)	Poisson's ratio v	Thermal expansion coefficient $1/^\circ c$	Conductivity $W/m^\circ c$
Aluminum	70	0.3	23×10^{-6}	204
Alumina	380	0.3	7.14×10^{-6}	10.4

The boundary conditions of the bottom and top surfaces of the plate are:

$$\tau_{rz} = 0, \quad \sigma_z = p_f(r,\theta,z), \quad \tau_{\theta z} = 0, \quad T_1 = 100^\circ c \qquad at \quad \varsigma = 0 \tag{36a}$$

$$\tau_{rz} = 0, \quad \sigma_z = -1GPa, \quad \tau_{\theta z} = 0, \quad T_2 = 500^\circ c \qquad at \quad \varsigma = 1 \tag{36b}$$

The values of geometric and other parameters are:

$$a = 1.0m, \quad s = 0.04, \quad f_1 = f_2 = 0.1, \quad k_1 = k_2 = 0.01, \quad p_1 = p_2 = 0.1, \quad \alpha_1 = \alpha_2 = 0.1 \tag{37}$$

Example 1: As a verification example, a uniform clamped supported FG circular plate carrying an asymmetric distributed transverse load considered previously by Nie and Zhong [19] is reexamined. For ease of comparison with this reference the same problem is considered and the same parameters ($E_0 = 380GPa, v = 0.3, h/a = 0.1, n_1 = 1$ and $\sigma_z = -1GPa$) are adopted.

Comparison of the present and Nie's results are shown in Tables 2. and 3 for the circumferential displacement V and transverse shear stress $\tau_{\theta\xi}$ at a location $\eta = 0.5$ and $\theta = 45^\circ$. Excellent agreement between the present results and those are given by Nie and Zhong can be seen in these tables.

Table2
Validity of the circumferential displacement V for uniform FG circular plate under asymmetric transverse load.

	ζ									
	0.0	0.1	0.2	0.3	0.5	0.6	0.7	0.8	0.9	1.0
(Nie & hong)	0.049	0.042	0.035	0.034	0.014	0.007	0.000	-0.002	-0.014	-0.021
present	0.048	0.041	0.034	0.035	0.013	0.008	0.000	-0.001	-0.015	-0.022

Table3
Validity of the transverse shear stress $\tau_{\theta\xi}$ for uniform FG circular plate under asymmetric transverse load.

	ζ									
	0.0	0.1	0.2	0.3	0.5	0.6	0.7	0.8	0.9	1.0
(Nie & Zhong)	0.000	0.302	0.565	0.771	1.033	1.062	1.023	0.812	0.471	0.000
present	0.000	0.301	0.5649	0.770	1.033	1.062	1.023	0.812	0.471	0.000

Example 2: Consider clamped supported non-uniform FG circular plate whose material properties and boundary conditions are mentioned in Eqs.(1)-(3) and (37). In this example, it is intended to investigate the temperature distribution along the thickness direction and the effect of thermal conductivity gradient index on temperature distribution. The top and bottom surfaces of the plate are ceramic and metal-rich, respectively. The temperature distribution simultaneous in radial and thickness directions is plotted in Fig. 2. It is seen from this Figure that the temperature distribution is nonlinear and its gradient at the bottom and top surfaces of the plate is considerably different. Fig. 3 shows the effect of thermal conductivity gradient index on temperature distribution along the transverse direction. It can be found from Fig. 3 that, the temperature in the thickness direction increases as the thermal conductivity gradient index increases. In addition the temperature curves converge to linear distribution when the index n_3 tends to zero, and $n_3 = 0$, corresponding to a homogeneous material.

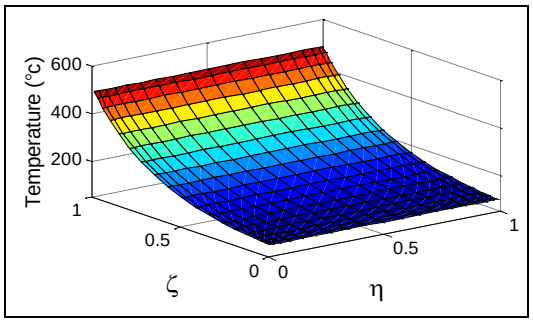

Fig.2
Distribution of temperature versus the dimensionless radial and thickness directions.

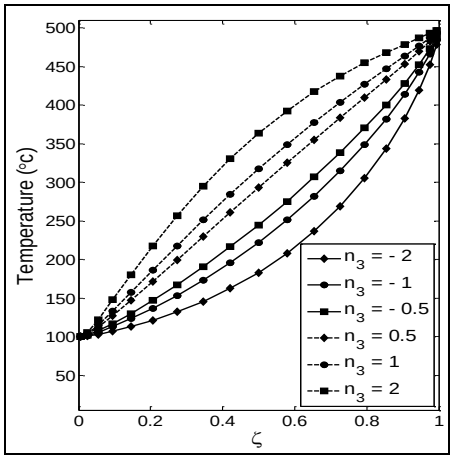

Fig.3
Distribution of temperature through the dimensionless thickness for different values of material constant n_3.

Example 3: In order to assess the convergence of the proposed DQ formulation, a non-uniform FG clamped circular plate resting on variable elastic foundations and placed in a uniform thermal field is considered. The boundary conditions and geometric parameters are the same as those in Example 2. Effect of the number of the

selected sample points on the convergence of the dimensionless transverse deflection W_b of the mid-radius point at $\theta = 60^\circ$ versus the number of the sample points N is presented in Table 4. for three types of loadings (e.g., mechanical, thermal and thermo-mechanical). From Table 4., it can be seen that the dimensionless transverse deflection of the mid-radius point of the plate approaches asymptotically to a specific value as the number of the discretization points increases beyond 10. Hence, present formulation converges with a high rate. In the present research, seventeen non-uniformly spaced discretization points are adopted.

Table4

Convergence of the dimensionless transverse deflection W_b against the number of DQ grid points for clamped supported FG circular plate.

Loading type	N								
	3	5	7	9	11	13	15	17	19
Mechanical	-0.045	-0.052	-0.054	-0.055	-0.056	-0.056	-0.056	-0.056	-0.056
Thermal	0.0046	0.0060	0.0068	0.0065	0.0065	0.0065	0.0065	0.0065	0.0065
Thermo-mechanical	-0.0068	-0.0098	-0.0099	-0.0097	-0.0096	-0.0096	-0.0096	-0.0096	-0.0096

Example 4: In the present example, a parametric study is performed to evaluate the thermo-elastic behavior of non-uniform FG clamped circular plate resting on variable elastic foundations and placed in a uniform thermal field. The geometric parameters and boundary conditions are the same as those in Example 2. The results for the Influences of different parameters (e.g., material properties graded indices, temperature difference between the lower and upper faces of the plate and trends of foundation stiffness variations) on displacements and stresses are plotted in Figs. 4 to 9. Moreover, the effect of thickness-to-radius ratio on the thermo-elastic response of the plate with various foundation patterns is shown in Table 5.

Table5

Magnitude of the transverse normal stress σ_{zb} in bottom surface of the plate at a point located at mid-radius of the plate and $\theta = 45^\circ$.

Foundation type		S							
		0.01	0.02	0.03	0.04	0.05	0.06	0.07	0.08
Uniform	$f_1 = f_2 = 0$	-0.489	-0.318	-0.222	-0.246	-0.299	-0.34	-8.332	-630.3
Linear	$f_1 = -0.1, f_2 = 0$	-0.483	-0.302	-0.202	-0.23	-0.287	-0.33	-8.219	-635.3
	$f_1 = 0.1, f_2 = 0$	-0.495	-0.332	-0.239	-0.26	-0.31	-0.349	-8.437	-625.6
Quadratic	$f_1 = f_2 = -0.1$	-0.478	-0.289	-0.186	-0.217	-0.277	-0.323	-8.154	-641.7
	$f_1 = f_2 = 0.1$	-0.498	-0.342	-0.251	-0.27	-0.317	-0.355	-8.489	-620.2

Influence of elastic gradient index on the displacements and stresses distribution along the thickness direction of a non-uniform solid circular FG plate at a location $\eta = 0.5, \theta = 45^\circ$ with gradient indices $n_1 = 0.25,\ 0.5, 0.75, 1$ and $n_2 = n_3 = 1$ is depicted in Fig.4. Gradient index Increases cause to increase V, W, σ_η and σ_Θ across the thickness of the plate. Fig. 4(c) shows that the distributions of transverse displacement change gradually from linear to the nonlinear form as n_1 increases. As the Figs.4 (b),(d) and (e) show, distribution of circumferential displacement, in-plane radial and tangential stresses ($V, \sigma_\eta, \sigma_\Theta$) along the thickness are more affected by the change of material gradient index. As the Fig. 4(f) shows, the transverse normal stress σ_ξ at one point is independent from variation of material gradient index. It transforms from tensile to compressive at the upper planes of the plate. It is easily seen from curves that shear stresses ($\tau_{\eta\xi}, \tau_{\theta\xi}$) satisfy fully the given mechanical boundary conditions, and the pick value of the stress $\tau_{\eta\xi}$ increases as n_1 increases. The stress $\tau_{\theta\xi}$ transforms from tensile to compressive at the overall thickness of the plate. Furthermore, the pick values of these stresses at compressive region enhance as grading index increases. Fig. 4(i) shows that the distributions of shear stresses $\tau_{\eta\theta}$ through the

thickness gradually change from linear to the nonlinear form as n_1 increases. An increase of transverse displacement through the thickness of the plate due to upward foundation pressure and temperature gradient in the same direction enhances the skin buckling of the plate.

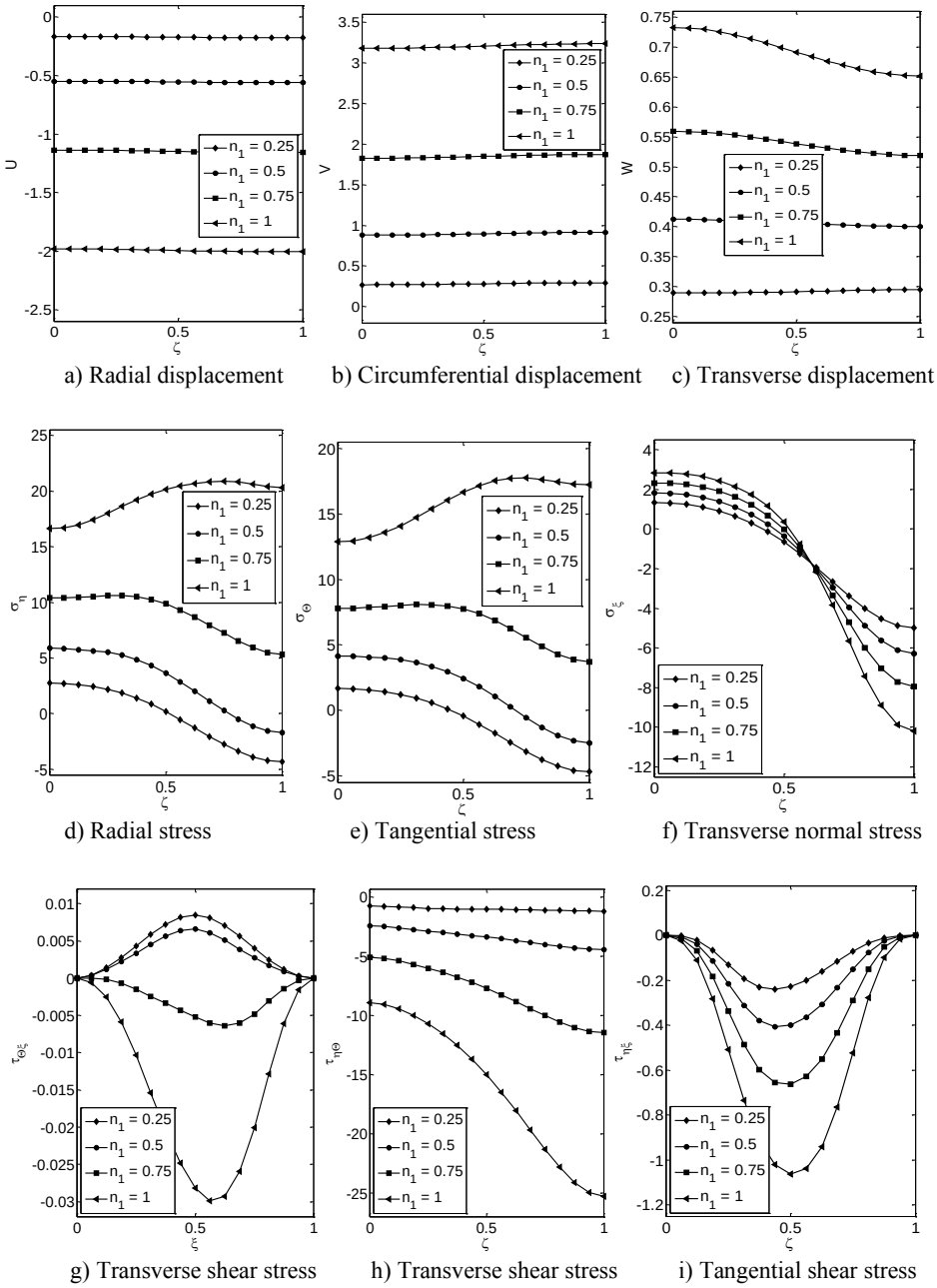

Fig.4
Effect of the material heterogeneity index on physical quantities across the plate thickness for a clamped circular plate at a location of radius midpoint and $\theta = 45°$.

Fig.5 presents the effect of thermal expansion gradient index on thermo-elastic behavior of mentioned plate with various gradient indices $n_2 = 0.25, 0.5, 0.75, 1$ and $n_1 = n_3 = 1$ at $\theta = 45°$ and radius midpoint. A quick glance at Fig. 5 reveals that the circumferential displacement and in-plane stress components ($\sigma_\eta, \sigma_\Theta, \tau_{\eta\theta}$) are strongly

affected by the change of n_2. Fig. 5(f) shows that the transverse normal stress component decreases along the thickness gradually and yields to the magnitude of thermo-mechanical tractions at top surface. Furthermore, this stress component at one point is independent from variation of thermal expansion gradient index. As discussed earlier, the distribution of transverse shear stresses ($\tau_{\eta\xi}, \tau_{\theta\xi}$) through the thickness of the plate shown in Figs.5 (g) and (h) satisfy the boundary conditions and transform from tensile to compressive throughout the thickness and moreover, the pick value of these stresses at compressive region enhances by the n_2 increases.

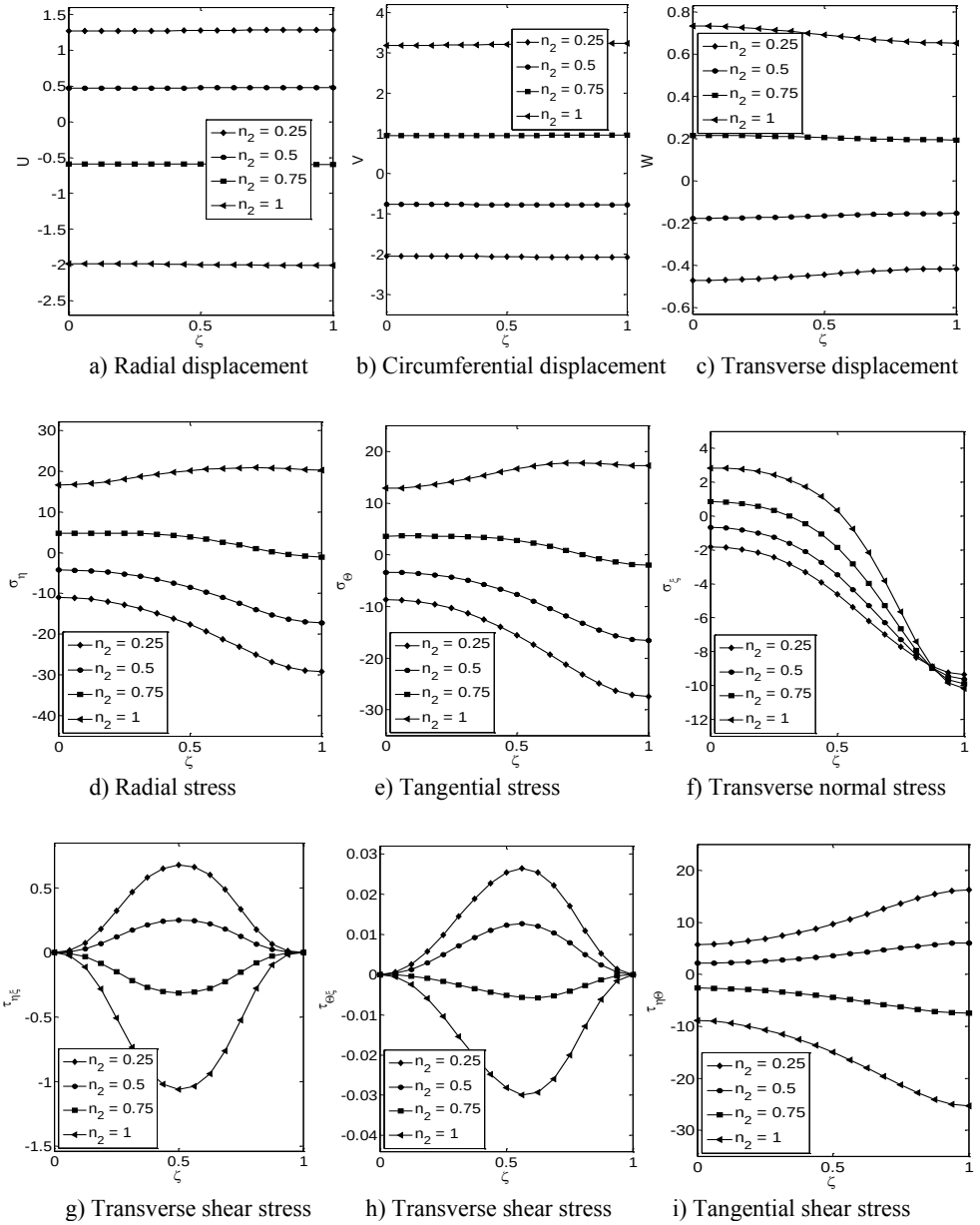

Fig.5
Effect of thermal expansion index on variation of mechanical entities across the plate thickness for a clamped circular plate at a location of radius midpoint and $\theta = 45°$.

Effect of the thermal conductivity gradient index on variation of mechanical entities across the plate thickness with $n_3 = 0.25, 0.5, 0.75, 1$ and $n_1 = n_2 = 1$ at $\eta = 0.5$ and $\theta = 45°$ is plotted in Fig.6. A quick glance at Fig. 6

demonstrates that the all displacement and stress components vary nonlinearly through the thickness of the plate. As the Figs. 6(d),(e) and (i) indicate, the in-plane stresses ($\sigma_\eta, \sigma_\Theta, \tau_{\eta\theta}$) through the thickness direction is more affected by the thermal conductivity gradient index variations at both surfaces specially at the upper surface. It is observable from Figs. 6(g) and (h) that the pick value of transverse shear stresses ($\tau_{\eta\xi}, \tau_{\Theta\xi}$) decreases as the gradient index n_3 increases.

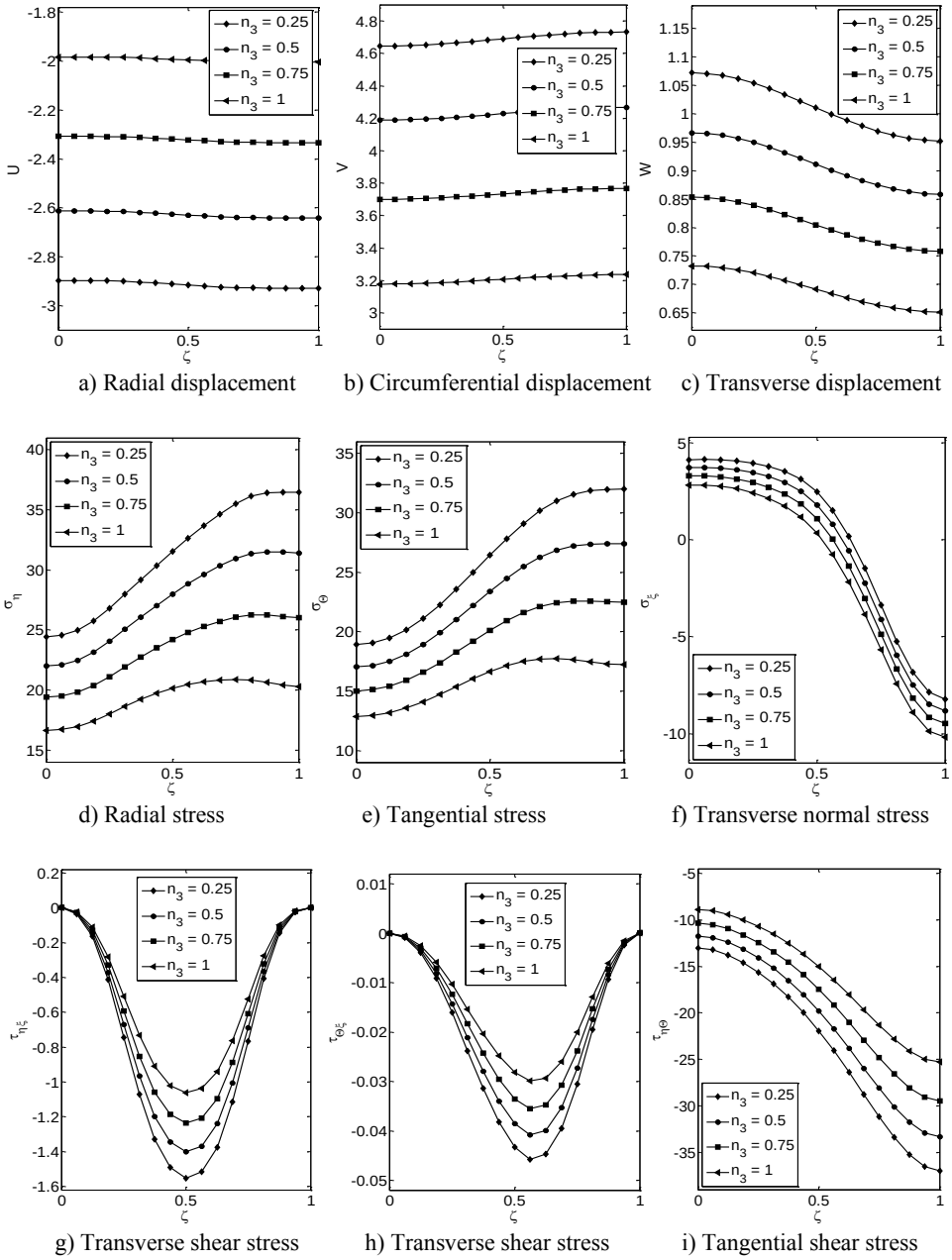

Fig.6
Effect of thermal conductivity index on variation of mechanical entities across the plate thickness for a clamped circular plate at a location of $\eta = 0.5$ and $\theta = 45°$.

Figs.7 (a) to (i) depict through-thickness distributions of the dimensionless stress and displacement components with various surfaces temperature conditions at $\theta = 30°$ and radius midpoint. Material properties gradient indices are

considered as $n_1 = 1n(E_h/E_0), n_2 = 1n(\alpha_h/\alpha_0)$ and $n_3 = 1n(k_h/k_0)$. As the figures display, all of mechanical quantities decreases when the surfaces temperature difference increases ($\Delta T = T_2 - T_1$ and $T_1 = 100^\circ c$). As the Fig. 7(e) shows, distribution of in-plain tangential normal stress (σ_Θ) along the thickness is remarkably affected by the plate faces temperature difference at both surfaces especially at the upper surface. As similar Figs. 4(f), 5(f) and 6(f) the transverse normal stress (σ_Θ) transform from tensile to compressive at the upper planes of the plate. It can be observed from Fig. 7(g) that the maximum value of transverse normal stress ($\tau_{\eta\xi}$) shifts from the mid surface toward the upper surface. As the Fig. 7(h) shows, the transverse shear stress ($\tau_{\Theta\xi}$) at one point is independent from variations of ΔT.

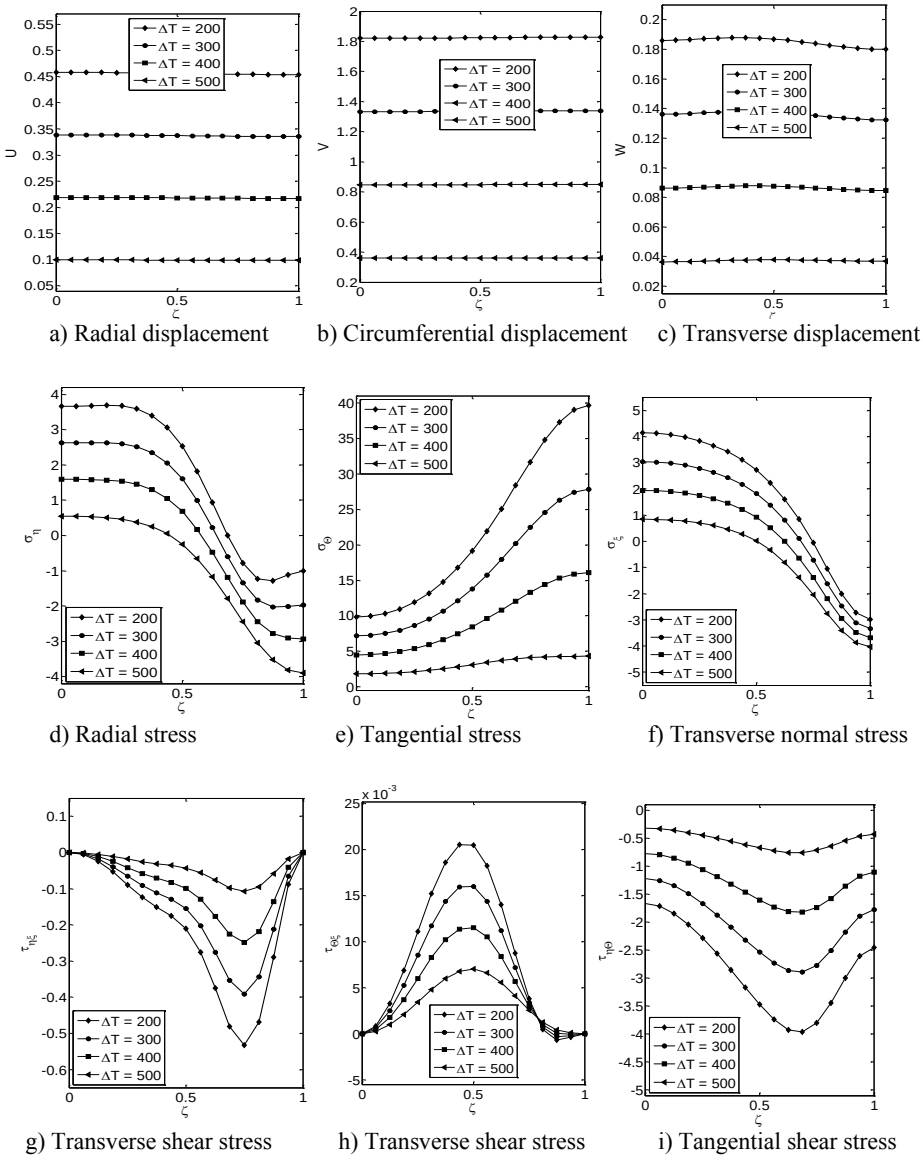

Fig.7
Effect of temperature difference on variation of mechanical entities across the plate thickness for a clamped circular plate at a location of $\eta = 0.5, \theta = 30^\circ c$ and $T_1 = 100^\circ c$.

Fig.8 presents the effect of foundation stiffness on thermo-elastic behavior of mentioned plate with indices $n_1 = 1n(E_h/E_0), n_2 = 1n(\alpha_h/\alpha_0), n_3 = 1n(k_h/k_0)$ at location $\eta = 0.5$ and $\theta = 30^\circ c$. It is evident from Figs.8 (a), (b) and (c) that the foundation coefficients increase causes to decrease *U,V* and *W* through the thickness of the plate. The normal pressure that exerted on the bottom surface of the plate has pressed the layers in the circumferential direction and caused a bending in the layers. For this reason, sing of the *V* component has changed. On the other hand, directions of the bending moments resulted from the foundation coupling and normal traction is not identical. Hence, the radial and hoop stresses have converted to compressive stresses and the transverse displacement distribution tends to a uniform distribution. Fig. 8(g) reveals that in the presence of thermal environment the influence of foundation coefficients on transverse shear stress is more pronounced in comparison with that of the normal traction. Therefore, enhance of the foundation-structure coupling interaction converts the parabolic distribution of the transverse shear stress at distinct regions to a somewhat linear one. Fig. 8(i) illustrates that the in-plane shear stress ($\tau_{\eta\Theta}$) at lower planes of the plate is independent from stiffness variations and strongly decreases with foundation coefficients increase at upper surfaces of the structure.

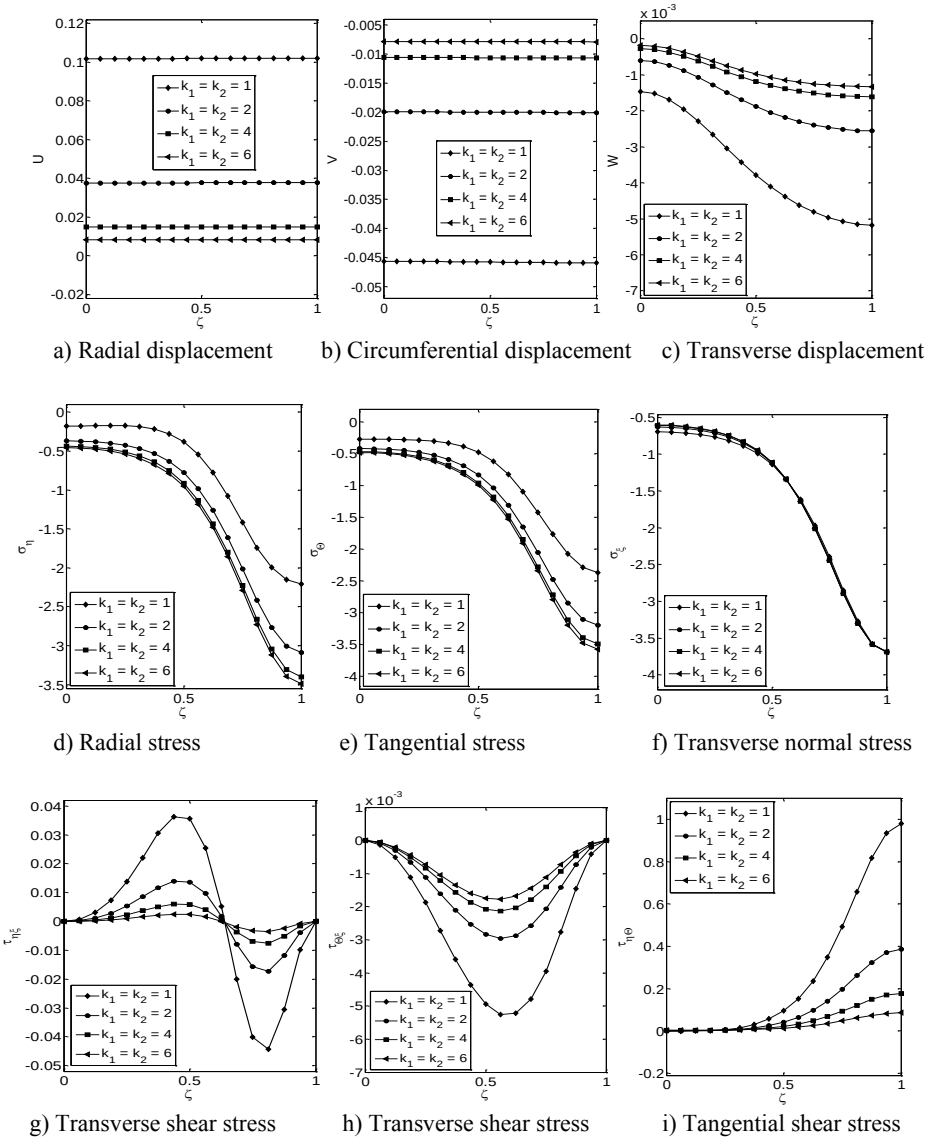

Fig.8
The effect of foundation coefficients on variation of mechanical entities across the plate thickness for a clamped circular plate at a location of $\eta = 0.5$ and $\theta = 30^\circ$.

Fig.9 displays the effect of foundation gradient indices on thermo-elastic behavior of clamped circular plate with nearly mentioned conditions and $f_1 = f_2 = 0.01, 0.1, 0.2, 0.3$. A quick glance at Fig. 9 reveals that the displacements (*U,V,W*) stresses ($\sigma_\eta, \sigma_\Theta, \sigma_\xi$) and the pick values of stresses ($\tau_{\eta\xi}, \tau_{\Theta\xi}, \tau_{\eta\Theta}$) increase through the plate thickness when the foundation gradient indices increases. It is observable from Figs. 9(c), (d) and (f) that the increases of foundation non-uniformity indices cause to additional bending moment due from foundation-structure coupling. Hence, the nature of displacement (*W*) and stresses ($\sigma_\Theta, \sigma_\xi$) have changed.

As a final stage, effect of the plate aspect ratio on thermo-elastic response of the plate is investigated and the resulted transverse normal stresses at the mid-radius point of the bottom surface of the plate are shown in Table 5. for various aspect ratios and different patterns of the elastic foundation. As it may be expected, when the aspect ratio increases, the plate stiffness increases and the edge reactions become more pronounced in comparison with the foundation reaction.

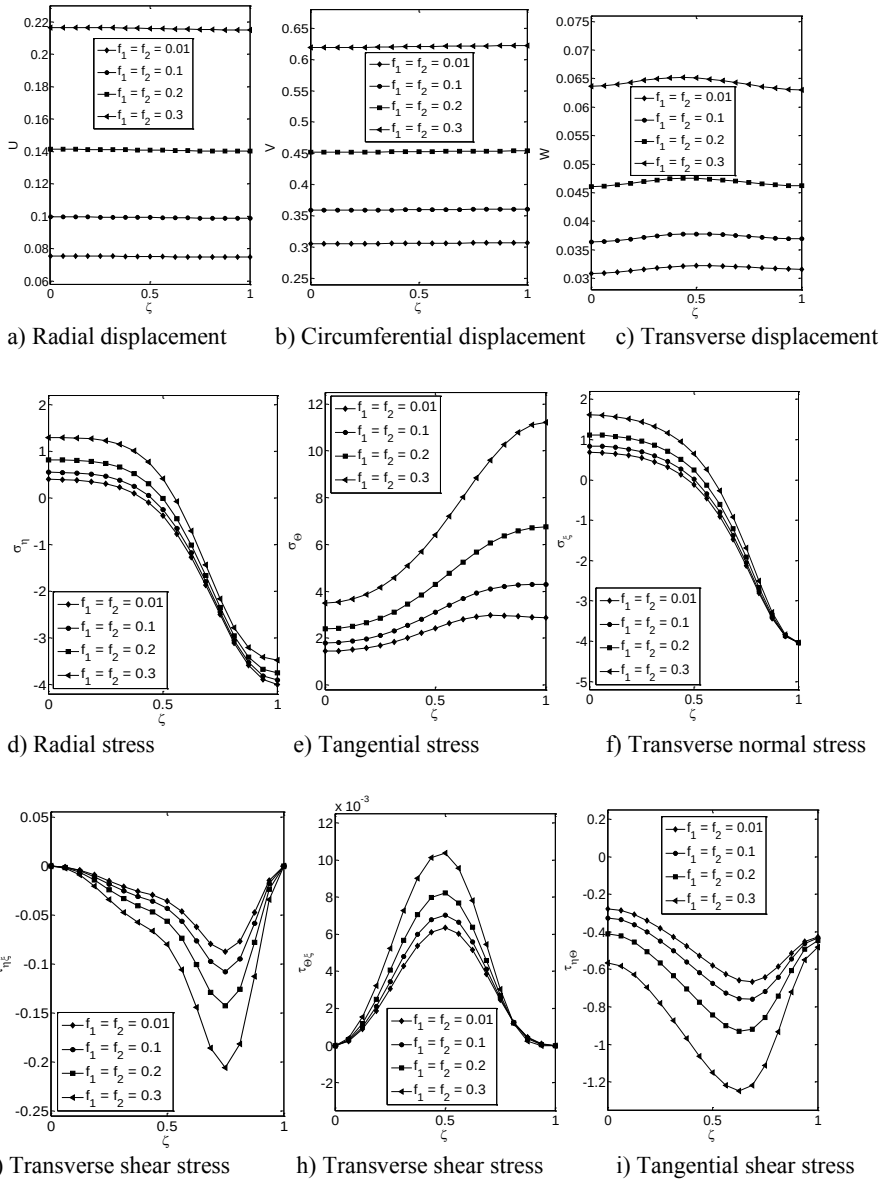

Fig.9
The effect of foundation graded indices on variation of mechanical entities across the plate thickness, for a clamped circular plate at a location of $\eta = 0.5$ and $\theta = 30^\circ$.

5 CONCLUSIONS

In the present study, uncoupled thermo-elastic theory is adopted to evaluate the three-dimensional deformations and stresses of functionally graded circular plate with variable thickness and resting on gradient elastic foundations subjected to thermo-mechanical loads. This means that the mechanical load has no contribution to the variation of the temperature. The thermo-elastic constants are assumed to be independent and vary exponentially through the thickness direction. The analysis is carried out by employing the state space method to express exactly the plate behavior along the graded direction and the one dimensional differential quadrature technique to approximate the radial variations of the parameters. The numerical results reveal that the material in homogeneities, the plate faces temperature difference and foundations parameters have an important effect on the distribution of the elastic field. On the other hand, the temperature gradient and the elastic medium (foundation) coupling effect may alter the nature of the stresses of the transversely loaded circular plate.

Some of the innovations incorporated in the present research are:

1. The proposed coupled method is especially useful to analyze the uncoupled thermo-elastic behavior of heterogeneous plate with more complicated geometry and boundary conditions.
2. Effects of the non-uniform elastic foundation parameters and thermal environment are considered in conjunction with the material heterogeneity to illustrate the elastic field components.
3. The proposed formulation and the presented results are comprehensive and cover many practical applications.
4. In contrast to the very limited works presented for the uncoupled thermo-elastic analysis of the variable thickness FG circular plates so far, the three dimensional stresses and deformations distribution through-the-thickness of the loaded plate are investigated. Furthermore, the mechanical loads may vary in an arbitrary pattern in the radial and circumferential directions.
5. The three dimensional theory presents an accurate prediction of three-axes Von-Misses stress, and as a result, it can accurately estimate the structure strength.
6. Results obtained in this paper may be considered as a more general case that include the combined effect of thermal load and multi mechanical tractions.

ACKNOWLEDGMENT

The author wishes to thanks from Mr. K. M. Majd as a scientific artist for his cooperation in preparing Fig. 1.

APPENDIX 1

The elements of state matrix at discretized points are

$$D_i = \begin{bmatrix} [0]_{N\times N} & [0]_{N\times N} & [0]_{N\times N} & [\delta_{ij}]_{N\times N} & [0]_{N\times N} & [0]_{N\times N} \\ [0]_{N\times N} & [0]_{N\times N} & [0]_{N\times N} & [0]_{N\times N} & [\delta_{ij}]_{N\times N} & [0]_{N\times N} \\ [0]_{N\times N} & [0]_{N\times N} & [0]_{N\times N} & [0]_{N\times N} & [0]_{N\times N} & [\delta_{ij}]_{N\times N} \\ [d_{ij}^{41}]_{N\times N} & [d_{ij}^{42}]_{N\times N} & [d_{ij}^{43}]_{N\times N} & [d_{ij}^{44}]_{N\times N} & [d_{ij}^{45}]_{N\times N} & [d_{ij}^{46}]_{N\times N} \\ [d_{ij}^{51}]_{N\times N} & [d_{ij}^{52}]_{N\times N} & [d_{ij}^{53}]_{N\times N} & [d_{ij}^{54}]_{N\times N} & [d_{ij}^{55}]_{N\times N} & [d_{ij}^{56}]_{N\times N} \\ [d_{ij}^{61}]_{N\times N} & [d_{ij}^{62}]_{N\times N} & [d_{ij}^{63}]_{N\times N} & [d_{ij}^{64}]_{N\times N} & [d_{ij}^{65}]_{N\times N} & [d_{ij}^{66}]_{N\times N} \end{bmatrix}_{6N\times 6N}$$

where $\delta_{ij}=0\ (i\neq j)\ ;\ \delta_{ii}=1$

$$d_{ii}^{41}=-\left(\frac{2(1-\nu)}{1-2\nu}\right)(s)^2\beta_{1i}^2\left(A_{ii}^{(2)}+\left(\frac{1}{\eta_i}+2\beta_{2i}\right)A_{ii}^{(1)}+\left((\frac{1}{\eta_i})\beta_{2i}+\beta_{3i}-\frac{1}{\eta_i^{\,2}}\right)\right)+(s)^2\beta_{1i}^2\frac{1}{\eta_i^2}\quad (i=j)$$

$$d_{ij}^{41}=-\left(\frac{2(1-\nu)}{1-2\nu}\right)(s)^2\beta_{1i}^2\left(\sum_{j=1}^{N}A_{ij}^{(2)}+\left(\frac{1}{\eta_i}+2\beta_{2i}\right)\sum_{j=1}^{N}A_{ii}^{(1)}\right)\quad (i\neq j)$$

$$d_{ii}^{42}=-\left(\frac{2\nu}{1-2\nu}\right)(s)^2\beta_{1i}^2\frac{1}{\eta_i}\left(A_{ii}^{(1)}+\beta_{2i}\right)+\left(\frac{2(1-\nu)}{(1-2\nu)}\right)(s)^2\beta_{1i}^2\frac{1}{\eta_i^2}-(s)^2\beta_{1i}^2\left(\frac{1}{\eta_i}A_{ii}^{(1)}+\left(\frac{\beta_{2i}}{\eta_i}-\frac{1}{\eta_i^2}\right)\right)\quad (i=j)$$

$$d_{ij}^{42}=-\left(\frac{1}{1-2\nu}\right)(s)^2\beta_{1i}^2\frac{1}{\eta_i}\sum_{j=1}^{N}A_{ij}^{(1)}\quad (i\neq j)\quad,\quad d_{ii}^{43}=-n_1 s\beta_{1i}\left(A_{ii}^{(1)}+\beta_{2i}\right)\quad (i=j)$$

$$d_{ij}^{43}=-n_1 s\beta_{1i}\sum_{j=1}^{N}A_{ij}^{(1)}\quad (i\neq j)\quad,\quad d_{ii}^{44}=-n_1\quad,\quad d_{ij}^{44}=0$$

$$d_{ii}^{46}=-\left(\frac{2\nu}{1-2\nu}\right)s\beta_{1i}\left(A_{ii}^{(1)}+\left(\beta_{2i}+\frac{1}{\eta_i}\right)\right)+\left(\frac{2\nu}{(1-2\nu)}\right)s\beta_{1i}\frac{1}{\eta_i}-s\beta_{1i}\left(A_{ii}^{(1)}+\beta_{2i}\right)\quad (i=j)$$

$$d_{ij}^{46}=-\left(\frac{1}{1-2\nu}\right)s\beta_{1i}\sum_{j=1}^{N}A_{ij}^{(1)}\quad (i\neq j)$$

$$d_{ii}^{51}=\left(\frac{2\nu}{1-2\nu}\right)s^2\beta_{1i}^2\frac{1}{\eta_i}\left(A_{ii}^{(1)}+\beta_{2i}\right)+\left(\frac{2(1-\nu)}{(1-2\nu)}\right)s^2\beta_{1i}^2\frac{1}{\eta_i^2}+s^2\beta_{1i}^2\left(\frac{1}{\eta_i}A_{ii}^{(1)}+\left(\frac{\beta_{2i}}{\eta_i}+\frac{1}{\eta_i^2}\right)\right)\quad (i=j)$$

$$d_{ij}^{51}=\left(\frac{1}{1-2\nu}\right)s^2\beta_{1i}^2\frac{1}{\eta_i}\sum_{j=1}^{N}A_{ij}^{(1)}\quad (i\neq j)$$

$$d_{ii}^{52}=-s^2\beta_{1i}^2\left(A_{ii}^{(2)}+\left(2\beta_{2i}+\frac{1}{\eta_i}\right)A_{ii}^{(1)}+\left(\beta_{2i}+\beta_{3i}-\frac{1}{\eta_i^2}\right)\right)+\left(\frac{2(1-\nu)}{1-2\nu}\right)s^2\beta_{1i}^2\frac{1}{\eta_i^2}\quad (i=j)\qquad (A.1)$$

$$d_{ij}^{52}=-s^2\beta_{1i}^2\left(\sum_{j=1}^{N}A_{ij}^{(2)}+\left(2\beta_{2i}+\frac{1}{\eta_i}\right)\sum_{j=1}^{N}A_{ij}^{(1)}\right)\quad (i\neq j)$$

$$d_{ii}^{53}=-n_1 s\beta_{1i}\frac{1}{\eta_i}\quad (i=j)\quad,\quad d_{ij}^{53}=0\quad (i\neq j)\quad,\quad d_{ii}^{55}=-n_1\quad (i=j)\quad,\quad d_{ij}^{55}=0\quad (i\neq j)$$

$$d_{ii}^{56}=-\frac{1}{\eta_i}\left(\frac{1}{1-2\nu}\right)\quad (i=j)\quad,\quad d_{ij}^{56}=0\quad (i\neq j)\quad,\quad d_{ii}^{61}=-n_1\left(\frac{\nu}{1-\nu}\right)s\beta_{1i}\left(A_{ii}+\left(\beta_{2i}+\frac{1}{\eta_i}\right)\right)\quad (i=j)$$

$$d_{ij}^{61}=-n_1\left(\frac{\nu}{1-\nu}\right)s\beta_{1i}\sum_{j=1}^{N}A_{ij}\quad (i\neq j)\quad,\quad d_{ii}^{62}=-n_1\left(\frac{\nu}{1-\nu}\right)s\beta_{1i}\frac{1}{\eta_i}\quad (i=j)\quad,\quad d_{ij}^{62}=0\quad (i\neq j)$$

$$d_{ii}^{63}=-\left(\frac{1-2\nu}{2(1-2\nu)}\right)s^2\beta_{1i}^2\left(A_{ii}^{(2)}+\left(\frac{1}{\eta_i}+2\beta_{2i}\right)A_{ii}^{(1)}+\left(\beta_{3i}+\frac{\beta_{2i}}{\eta_i}-\frac{1}{\eta_i^{\,2}}\right)\right)\quad (i=j)$$

$$d_{ij}^{63}=-\left(\frac{1-2\nu}{2(1-2\nu)}\right)s^2\beta_{1i}^2\left(\sum_{j=1}^{N}A_{ij}^{(2)}+\left(\frac{1}{\eta_i}+2\beta_{2i}\right)\sum_{j=1}^{N}A_{ij}^{(1)}\right)\quad (i\neq j)$$

$$d_{ii}^{64}=-\left(\frac{\nu}{(1-\nu)}\right)s\beta_{1i}\left(A_{ii}+\frac{1}{\eta_i}\left(\beta_{2i}+\frac{1}{\eta_i}\right)\right)\quad (i=j)\quad,\quad d_{ij}^{64}=-\left(\frac{\nu}{(1-\nu)}\right)s\beta_{1i}\sum_{j=1}^{N}A_{ij}^{(1)}\quad (i\neq j)$$

$$d_{ii}^{65}=-\frac{1}{2(1-\nu)}\frac{s\beta_{1i}}{\eta_i}\quad (i=j)\quad,\quad d_{ij}^{65}=0\quad (i\neq j)\quad,\quad d_{ii}^{66}=-n_1\quad (i=j)\quad,\quad d_{ij}^{66}=0\quad (i\neq j)\qquad \text{i = 1,2,3,… , N}$$

The elements of temperature coefficient matrix at sample points are

$$B_i = \begin{bmatrix} [0]_{N\times N} & [0]_{N\times N} & [0]_{N\times N} & [0]_{N\times N} & [0]_{N\times N} & [0]_{N\times N} \\ [0]_{N\times N} & [0]_{N\times N} & [0]_{N\times N} & [0]_{N\times N} & [0]_{N\times N} & [0]_{N\times N} \\ [0]_{N\times N} & [0]_{N\times N} & [0]_{N\times N} & [0]_{N\times N} & [0]_{N\times N} & [0]_{N\times N} \\ [0]_{N\times N} & [0]_{N\times N} & [0]_{N\times N} & [0]_{N\times N} & [0]_{N\times N} & [0]_{N\times N} \\ [0]_{N\times N} & [0]_{N\times N} & [0]_{N\times N} & [0]_{N\times N} & [0]_{N\times N} & [0]_{N\times N} \\ \left[b_{ij}^{61}\right]_{N\times N} & [0]_{N\times N} & [0]_{N\times N} & [0]_{N\times N} & [0]_{N\times N} & \left[b_{ij}^{66}\right]_{N\times N} \end{bmatrix}_{6N\times 6N} \tag{A.2}$$

$$b_{ii}^{61} = \frac{(n_1+n_3)(1+\nu)}{1-\nu}\left(\frac{\alpha_0}{\alpha_3}\right) \ (i=j),\ b_{ij}^{61}=0 \quad (i\neq j)$$

$$b_{ii}^{66} = \frac{(1+\nu)}{1-\nu}\left(\frac{\alpha_0}{\alpha_3}\right) \ (i=j),\ b_{ij}^{66}=0 \quad (i\neq j) \qquad \text{i , j = 1,2,3,... , N}$$

REFERENCES

[1] Reddy J.N., Wang C.M., Kitipornchai S., 1999, Axisymmetric bending of functionally graded circular and annular plates, *European Journal of Mechanics A/Solids* **18**(2): 185-189.

[2] Najafizadeh M. M., Heydari H. R., 2008, An exact solution for buckling of functionally graded circular plates based on higher order shear deformation plate theory under uniform radial compression, *International Journal of Mechanical Science* **50**(3): 603-612.

[3] Ma L. s., Wang T. J., 2003, Nonlinear bending and post buckling of functionally graded circular plates under mechanical and thermal loadings, *International Journal of Solids & Structures* **40**: 3311-3330.

[4] Khorshidvand A. R., Jabbari M., Eslami M. R., 2012, Thermo elastic buckling analysis of functionally graded circular plates integrated with oiezoelectric layers, *Journal of Thermal Stress* **35**: 695-717.

[5] Kiani Y., Eslami M. R., 2013, An exact solution for thermal buckling of annular FGM plates on an elastic medium, *Composites Part: B Engineering* **45**: 101-110.

[6] Gaikwad K. R., 2013**,** Analysis of thermo-elastic deformation of a thin hollow circular disk due to partially distributed heat supply, *Journal of Thermal Stress* **36**: 207-224.

[7] Golmakani M.E., Kadkhodayan M., 2014, An investigation into the thermo elastic analysis of circular and annular FGM plates, *Mechanics of Advanced Materials and Structures* **21**(1): 1-13.

[8] Fallah F., Noseir A., 2015, Thermo - mechanical behavior of functionally graded circular sector plates, *Acta Mechanica* **226**: 37-54.

[9] Gunes R., Reddy J. N., 2008, Nonlinear analysis of functionally graded circular plates under different loads and boundary conditions, *International Journal of Structural Stability and Dynamic* **8**(1): 131-159.

[10] Prakash T., Ganapathi M., 2006, Asymmetric flexural vibration and thermo-elastic stability of functionally graded circular plates using finite element method, *Composite Part: B Engineering* **37**(7-8): 642-649.

[11] Gomshei M. M., abbasi V., 2013, Thermal buckling analysis of annular FGM plate having variable thickness under thermal load of arbitrary distribution by finite element method, *Journal of Mechanical Science and Technology* **27** (4): 1031-1039.

[12] Afsar A. M., Go J., 2010, Finite element analysis of thermo-elastic field in a rotating FGM circular disk, *Applied Mathematical Modeling* **34**: 3309-3320.

[13] Leu S-Y., Chien L-c., 2015, Thermoelastic analysis of functionally graded rotating disks with variable thickness involving non-uniform heat source, *Journal of Thermal Stress* **38**: 415-426.

[14] Safaeian Hamzehkolaei N., Malekzadeh P., Vaseghi J., 2011, Thermal effect on axisymmetric bending of functionally graded circular and annular plates using DQM, *Steel and Composite Structures* **11**(4): 341-358.

[15] Malekzadeh P., Golbahar Haghighi M.R., Atashi M.M., 2011, Free vibration analysis of elastically supported functionally graded annular plates subjected to thermal environment, *Meccanica* **47**(2): 321-333.

[16] Sepahi O., Forouzan M.R., Malekzadeh P., 2011, Thermal buckling and post buckling analysis of functionally graded annular plates with temperature dependent material properties, *Materials & Design* **32**(7): 4030-4041.

[17] Sepahi O., Forouzan M.R., Malekzadeh P., 2010, Large deflection analysis of thermo-mechanical loaded annular FGM plates on nonlinear elastic foundation via DQM, *Composite Structures* **92**: 2369-2378.

[18] Jabbari M., Shahryari E., Haghighat H., Eslami M.R., 2014, An analytical solution for steady state three dimensional thermo elasticity of functionally graded circular plates due to axisymmetric loads, *European Journal of Mechanics A/Solids* **47**: 124-142.

[19] Nie G.J., Zhong Z., 2007, Semi-analytical solution for three-dimensional vibration of functionally graded circular plates, *Computational Methods in Applied Mechanics and Engineering* **196**: 4901-4910.

[20] Yu Li X., Li P.D., Kang G.Z., Pan D.Z., 2013, Axisymmetric thermo-elasticity field in a functionally graded circular plate of transversely isotropic material, *Mathematics and Mechanics of Solid* **18**(5): 464-475.

[21] Behravan Rad A., 2012, Semi-analytical solution for functionally graded solid circular and annular plates resting on elastic foundations subjected to axisymmetric transverse loading, *Advances in Applied Mathematics and Mechanics* **4**(2): 205- 222.

[22] Behravan Rad A., Alibeigloo A., 2013, Semi-analytical solution for the static analysis of 2D functionally graded circular and annular circular plates resting on elastic foundation, *Mechanics of Advanced Materials and Structures* **20**(7): 515-528.

[23] Behravan Rad A., 2012, Static response of 2D functionally graded circular plate with gradient thickness and elastic foundations to compound loads, *Structural Engineering and Mechanics* **44**(2):139-161.

[24] Shu C., 2000, *Differential Quadrature and Its Application in Engineering*, Springer, New York.

[25] Zong Z., Zhang Y., 2009, *Advanced Differential Quadrature Methods*, CRC Press, New York.